nature geoscience

SUPPLEMENTARY INFORMATION

DOI: 10.1038/NGEO1800

"Warming-induced increase in aerosol number concentration likely to moderate climate change"

by Paasonen, P. *et al*.

Supplementary Methods

Detailed site descriptions

Hyytiälä: The SMEAR II atmospheric observatory is located in Southern Finland (61°51'N, 24°70' E, 181 m above the sea level), approximately 60 kilometres distance from the closest major city[31]. The air quality at the site is considered to represent typical regional background conditions for higher latitudes of Europe. The air masses are influenced by European long range transport but at times very clean Arctic air is observed. The station is located within a Scots pine stand.

Värriö: The subarctic SMEAR I atmospheric observatory is located in a remote location in Northern Finland (67°46'N, 29°35'E, 390 m a.s.l.)[32]. The station is characterized by prevailing extremely clean environment, with intermediate long range transport from Kola Peninsula and Southern Finland. The station is located within a Scots pine stand.

Vavihill: The EMEP/ACTRIS field station (56° 01' N, 13° 09' E, 172 m a.s.l.) is situated in a rural environment in the southern part of Sweden with no local sources of pollution[33]. The closest cities are Helsingborg, Copenhagen and Malmö, at the distance of 25 km to west, 40 km to southwest and 45 km to south-southwest, respectively.

Melpitz: The station is an ACTRIS atmospheric research station in Eastern Germany (51°32'N, 12°54'E, 87 m a.s.l.) 40 km northeast of Leipzig[34]. The station is surrounded by flat and semi-natural grasslands without any obstacles, as well as agricultural pastures and forests in wider environment. Atmospheric observations at Melpitz can be regarded as representative of regional background conditions in Central Europe.

Hohenpeissenberg: The Meteorological Observatory Hohenpeissenberg (MOHp, 47°48' N, 11°07'E, 980 m a.s.l.) is a Global Atmosphere Watch (GAW) site and mountain station operated by the German Weather Service (DWD)[35]. The observatory is located on top of the Hohenpeissenberg mountain and about 300 m above the surrounding countryside. The nearest major city, Munich, is distant at ca. 60 km. MOHp is surrounded mainly by forests and agricultural pastures with coniferous trees and beeches growing on the slopes of the Hohenpeissenberg mountain in most directions.

K-puszta: The K-puszta station (46°58'N, 19°33'E, 136 m a.s.l.) is a rural site about 15 km northwest from the nearest town Kecskemét (70 000 inhabitants) and 80 km southeast of Budapest (1.7 million inhabitants)[36]. The station is located on a forest clearing; the surrounding forest contains both deciduous and coniferous trees. The EUSAAR/ACTRIS station has been involved in the GAW network and the European Monitoring and Evaluation Program.

San Pietro Capofiume: The station (44°39'N, 11°37'E) is located about 30 km northeast from the city of Bologna, in the Po Valley, the largest industrial, trading and agricultural area in Italy with a high population density[37]. The station itself is in a sparsely inhabited area open to Adriatic Sea to the east side, but enclosed by densely populated areas, on its southern, western and northern sides. There are power plants and industrial areas along the Po River and close to the harbours of Venice and Ravenna.

Yakutsk: The Spasskaya Pad forest research station is located (62°15'N, 129°14'E, 220 m a.s.l.) about 30km north of Yakutsk city, and the site is representative for the vast forested areas in eastern Siberia[38]. The station is run by the Institute for Biological Problems of Cryolithozone, SB RAS, Yakutsk. The most abundant tree species in eastern Siberia is larch (Larix cajanderi) which in large areas, like in Yakutsk, grow on permafrost soil.

Morgan Monroe State Forest: The station (39.317°N, 86.417°W) is located in an expansive deciduous forest (of > 95 km^2) within a relatively polluted continental region in which there are many stations that fail National Ambient Air Quality Standards for ozone and particulate matter[39]. The tree total basal area is approximately 26 $m^2\ ha^{-1}$ and is dominated by five species: sugar maple (Acer saccharum, 27%), tulip poplar (Liriodendron tulipifera, 19%), sassafras (Sassafras albidum, 9.5%), white oak (Quercus alba, 9%), and black oak (Quercus nigra, 8.5%).

Egbert: The measurements were made at the Centre for Atmospheric Research Experiments of Environment Canada in Egbert, Ontario (44.2325°N, 79.78139°W, 251 m a.s.l.). The site is approximately 75 km north-northwest of Toronto, Ontario in a rural area of mixed forest and farmland[40]. The predominant wind direction is westerly, but the site often receives air from the sparsely populated and heavily forested regions to the north (mix of coniferous and broadleaf species; http://cfs.nrcan.gc.ca) as well as from the south where air arrives from the heavily populated regions of Southern Ontario and the Northern US.

Botsalano: The Botsalano game reserve (25°32'28 S, 25°45'16 E, 1424 m a.s.l.) is a clean background savannah site with relatively low pollutant concentrations, occasionally hit by plumes from Johannesburg and Rustenburg areas[41]. The annual precipitation amount is 540 mm yr^{-1} of which approximately 60% comes during the summer. Typical winter temperatures vary between 4 and 20 °C, the summer temperatures being between 17 and 31 °C. The vegetation of

the reserve is fairly homogeneous dry busveld, typical of a savannah biome. The seasonal activity of vegetation is governed by the precipitation available similar to other dry ecosystems. In contrast to the other studied sites, around which isoprene emissions are either smaller or comparable to monoterpene emissions[42], around the Botsalano site the isoprene emissions have been estimated to be dominant[43].

Particle number size distribution measurements

The dry aerosol number size distributions were obtained using mobility particle size spectrometers, which all use electrical mobility to size-select the particles[44]. The Differential Mobility Particle Sizer (DMPS) and the Scanning Mobility Particle Sizer (SMPS) measure aerosol particle number size distributions by first drying and neutralizing the aerosol sample, and then using a cylindrical differential mobility analyser to select a narrow particle diameter range[45]. The almost monodisperse aerosol is then detected using a Condensational Particle Counter (CPC) instrument. The size range and number of size channels varied from site to site. Difference between DMPS and SMPS is the mode of operation: DMPS measures one size channel for a moment before moving to the next one, SMPS continuously varies the voltage in the mobility analyser. The Fast Mobility Particle Sizer (FMPS 3091, TSI, Inc, applied at Morgan Monroe State Forest) measures aerosol particle concentrations in 32 logarithmically spaced size channels from 6.04 to 523.3 nm using an electrical mobility measurement technique similar to that used in SMPS[46]. However, instead of a CPC, the FMPS spectrometer uses multiple, low-noise electrometers for particle detection.

Note on the calculation of the columnar boundary layer burden

The times when the re-analysis boundary layer height (BLH) was below 30 m were excluded from the analysis. In case of Morgan Monroe State Forest, where the measurements were conducted at 47 m above the ground level, the lowest BLH value utilized was 70 m, and in case of Hohenpeissenberg, where the station is on a mountain over 300 m above the surrounding environment, the lowest BLH value utilized was 400 m. Due to availability reasons, BLH at Yakutsk was adapted from NCEP GDAS database.

Statistical significance of concentration and burden temperature dependence

We estimated the statistical significance of the relationships between N_{100}, B_{100} and air temperature using an autoregressive model of the measured concentrations and temperatures. The time series of observations were split into two parts: below and above 5°C. We then calculated the log-linear regression coefficients between log(N_{100}) and T and log(B_{100}) and T for higher temperature time series, obtaining the slopes (s) of the observed temperature dependence. Using the lower temperature time series, the 1-autoregression coefficient (α) and standard deviation (σ) of the concentrations and burdens were estimated. Using these parameters, we generated 10000 samples of randomized N_{100} and burden time series, using daily AR(1) model

$$x(i) = x(i-1)\alpha + \sigma e(i) \quad (1)$$

where x is either N_{100} or B_{100} and e(i) is random Gaussian noise. The first value of x and values after a data gap were initialized with a random value (σe). We then combined these randomized AR(1) time series with whole measured temperature time series and calculated log-linear regression slopes (s_r) of the >5°C part of the random realizations. We then estimated the

statistical significance of the original regression slopes by observing how many of the randomized AR(1) time series produced at least as large log-linear regression slopes as the original sample (i.e. number of instances where $s_r \geq s$ divided by 10000 samples).

The results are shown in Table S1. The N_{100}-T slopes at T>5°C are unlikely ($p \leq 0.01$) to be formed by random process at 8 of the 11 stations. Based on this test, all of the B_{100}-T slopes are statistically significant with a confidence level p<0.001.

Size-resolved Pan-European anthropogenic particle number inventory

A size-resolved inventory for European anthropogenic particle number (PN) emissions in year 2005 was developed in the framework of EU FP6 EUCAARI[19,47]. The PN inventory covers emissions of all particles in the 10-300 nm size range, thus capturing the majority of PN emissions. The ~70 source categories distinguished in the underlying database are aggregated to 10 major source sectors. Unique size resolved PN emission factors were collected for each source sector. The total European annual PN emissions excluding international shipping were estimated to be $19 \cdot 10^{26}$ (particles per year) and dominated by transport, residential combustion and industrial processes. The share of source sectors varies considerably over the domain reflecting regional differences in emission reduction policies, technologies, fuel quality and use of solid fuels for small scale combustion. The emission inventory is gridded at a high spatial resolution of (1/8)° x (1/16)° longitude – latitude (~ 7 x 7 km^2). A distinction is made in the gridding between point and area sources. Point source emission is distributed according to location, capacity and fuel type (when applicable). Area sources are distributed using distribution maps of proxy data such as population density and traffic intensity. Particular attention has been given to the spatial distribution of transport emission and emission due to residential combustion.

For modelling purposes weekly, daily and hourly factors were constructed to breakdown annual total emissions into hourly emissions[48].

We estimated the burden related to anthropogenic emissions from the total annual emissions of > 100 nm particles taken from the PN inventory in ca. 200 x 200 km^2 area surrounding the measurement site. These emissions were converted to average daily emissions per m^2, and the burden was calculated (assuming steady-state) by multiplying the average daily emissions with the approximated lifetime of accumulation mode particles, 5 days. The minimum and maximum values for the bars in Fig. 2b of the main article were produced by multiplying the average burden with cumulative minima and maxima of monthly, daily and hourly factors described above.

Estimation of total annual contribution of natural production of > 100 nm particles

The temperature dependent production of particles larger than 100 nm in diameter was calculated with the temperature information around Europe in year 2005 from NCEP/DOE AMIP-II Reanalysis 2 database (with 3 h time resolution). From this data we calculated burden B_{100} as a function of location and time with $B_{100}(\text{lat},\text{lon},t)=10^{\wedge}(10.82+0.05*T(\text{lat},\text{lon},t)/°\text{C})$ m^{-2} from the exponential fit made to Fig. 2b. Assuming steady-state, this burden was converted to source rate of >100 nm particles by dividing it with estimated particle life-time of 5 days. The source rate was set to zero when the temperature was below 5 °C. Finally the annual production of >100 nm particles was calculated by summing over the whole year.

The temperature dependent production was compared to the direct anthropogenic emissions of >100 nm particles from the Size-resolved Pan-European anthropogenic particle number

inventory (see previous chapter). As the spatial resolution of this emission inventory ((1/8)° x (1/16)°) is much higher than that of NCEP Reanalysis 2 database (1.875° x 0.952°), we summed the annual anthropogenic emissions from the inventory within the grid cells of the NCEP Reanalysis 2 database. In order to take into account only the land area, we made the comparison between the sums of the temperature dependent productions and anthropogenic emissions from those NCEP Reanalysis 2 grid cells that included more than 5000 emission inventory grid cells or point sources (the mode value being around 5500).

The percentage calculated for the contribution of the temperature dependent natural growth mechanism to the total production of >100 nm particles from continental Europe (assuming transport from outside Europe and direct biogenic emissions of >100 nm particles to be negligible) was 45 %.

Monoterpene concentration measurements

Proton Transfer Reaction Mass Spectrometer (PTR-MS, Ionicon Analytik GmbH, Innsbruck, Austria) applied for monoterpene concentration measurements in Hyytiälä and Yakutsk allows on-line measurements of volatile organic compounds (VOC) with concentrations of a few ppt. The method is based on reactions of hydronium (H_3O^+) ions, which perform non-dissociative proton transfer to most of the common volatile organic compounds but do not react with any of the components present in clean air. The set-up consists of a discharge ion source to produce H_3O^+ ions, a drift-tube reactor, where the proton transfer reaction between H_3O^+ and the target VOC take place and a quadrupole mass spectrometer for the detection of reagent and product ions. Since PTR-MS measures only masses, different compounds with same mass cannot be distinguished and it cannot be used for identification of measured compounds. A detailed

description of PTR-MS technique is given by Lindinger et al.[49] and de Gouw and Warneke[50]. The volume mixing ratio calculations and calibration procedure are described in Taipale et al.[51]. Measurements and quality assurance at the Yakutsk location followed the protocol given in Holst et al.[52].

At the Hohenpeissenberg observatory Gas Chromatography Mass Spectrometer (GC-MS) measurements of C5 to C10 hydrocarbons including speciated monoterpenes were conducted within the Global Atmospheric Watch (GAW) programme in year 2000 through the day with high time resolution (< 1 h) and during 2007 and 2008 daily at 1:00 and 13:00 CET[53]. Sampling includes ozone removal and adsorptive trapping on Tenax TA and Carbopack B. The analytical system includes a cryo-focussing step for narrow injection bands, separation on a non-polar capillary column and parallel detection by FID (flame ionisation detection) and ion trap mass spectrometer. The Hohenpeissenberg system has been thoroughly tested with various terpene mixtures and standard addition measurements. Though some artefacts were observed for several terpenes, they generally did not exceed 30%[54]. Overall, the accuracies (2-σ) of most of the analysed NMHCs are better than 20% or a few pptv.

The total monoterpene concentration utilized in this article is a sum of all the monoterpene concentrations measured with the GC-MS (α-thujene, tricyclene, α-pinene, camphene, propylbenzene, sabinene, myrcene, β-pinene, α-phellandrene, 3-carene, α-trepinene, p-cymene, limonene, β-phellandrene).

Aerosol Mass Spectrometer (AMS)

The Aerodyne Aerosol Mass Spectrometer (AMS, Aerodyne Research Inc., Billerca, U.S.) measures the chemical composition of aerosol particles using time-of-flight mass spectrometry[12]. It features an aerodynamic lens for concentrating the aerosol particles into a narrow beam, a particle time-of-flight chamber for particle size distribution measurement, thermal vaporization of the sample at 600°C, 70 eV electron impact (EI) ionization of the produced vapour and a time-of-fight mass spectrometer (ToF-MS) to obtain a mass spectrum for the ions. The mass spectra of ions is interpreted, using knowledge of 70 eV EI molecular fragmentation patterns, in order to assign the aerosol mass into subgroups of different chemical composition; sulphates, organics, nitrates, ammonium and chlorides. The measured mass loadings are corrected for collection efficiency, to make the results comparable with other aerosol instrumentation. The AMS does not quantitatively see "non-refractory" compounds, i.e. those that are not vaporized under 600 °C, such as sea salt and black carbon. Particulate water is also not quantitatively measured and is not included in AMS total mass.

Effect of precipitation and radiation on the mixed layer N_{100} burdens

In order to estimate the effect of precipitation on our results, we repeated the analysis of the temperature dependence of the aerosol number burden, B_{100} (presented in the main article), for those stations from where the precipitation data were available, separating the periods during precipitation and when no precipitation took place. The results depicted in Fig. S2 show that the dependency of B_{100} on temperature is not conditional on the occurrence of precipitation.

Since the air temperature and short-wave radiation are strongly correlated (R^2 = 0.43 for midday values in Hyytiälä), we tested which one of these two quantities has more influence on the increase in B_{100}. In Figure S3 B_{100} is presented as function of temperature and radiation for those eight measurement sites from which the global radiation data was available. Especially at the stations in which the burden varies the most and is least affected by anthropogenic emissions (Hyytiälä, Värriö, Morgan Monroe S. F. and Egbert) the change in B_{100} follows the change in air temperature, whereas the level of global radiation did not seem to have strong effect on the observed burden. Based on this analysis it seems clear that the primary driving force behind the B_{100} increase is air temperature and not radiation. The inference drawn from this analysis is thus that B_{100} is more strongly determined by variations in precursor emissions (as dictated by air temperatures) than oxidation chemistry (as determined by radiation receipt).

On the temperature dependencies and correlations of N_{100}, m_{OA} and [MT]

Fits to N_{100} vs [MT] in Fig. 3 of the main article were determined with a bivariate fitting method[55] to logarithmic values of N_{100} and [MT]. The variances of log(N_{100}) and log([MT]) in each data point required for fitting were set equal, i.e. the relative variations in N_{100} and [MT] were taken as equally effective. Even though this is a simplification, it is better than assuming no variation in one of the axes, which would be the case in linear least squares fitting. The regression uncertainty for N_{100} vs [MT] was approached via pairwise moving block bootstrap (PVMBB) method described in Mudelsee, (2010)[56] algorithm 8.1, with block length selection from Eq. 7.32 in the same reference, and using the bivariate fitting method mentioned above[55]. The datasets were assumed to be individually homoscedastic, and the ratio of their noise components (derived from one-pass pre-whitening routine) was used in the fit residual definition.

This method conserves the autoregression of the individual timeseries, and from 1000 bootstrap iterations, the 5th and 95th percentiles of the PVMBB fit parameters were taken as the confidence interval of the regression parameters.

The lower correlation between N_{100} and [MT] than that between N_{100} and m_{oa} might be attributable to a time-delay necessary to generate lower volatility condensable products from the parent monoterpenes and on the lifetime differences. Correlations are also naturally weakened if some other VOCs besides monoterpenes are significant components in the condensation. Furthermore, the correlation between N_{100} and [MT] is probably affected with continuously emitted monoterpenes concentrating during night-time conditions with smaller BL heights after the sunset, whereas a similar increase in concentrations is not presumable for aerosol particles for which horizontal advection is typically a more effective source than emissions.

The temperature dependencies of the mass of organic aerosol (m_{OA}, Fig. S5a), monoterpene concentration ([MT], Fig. S5b) and CCN-sized particle number concentration (N_{100}) are all exponential. Results of the least squares regression fits to $m_{OA} = \alpha_{OA}$*exp(β_{OA} T/°C) for Hyytiälä and Egbert data, to [MT] = α_{MT}*exp(β_{MT} T/°C) for Hyytiälä, Yakutsk and Hohenpeissenberg data, and to $N_{100} = \alpha_{N}$*exp(β_{N} T/°C) for Hyytiälä, Egbert, Yakutsk and Hohenpeissenberg data are presented in Table S2. The confidence intervals for these (log to linear) least squares fits were done using moving block bootstrap similarly as for N_{100} vs [MT] (described earlier), but with univariate residual definition from the fitted parameter. The similarity of the temperature dependencies in terms of the values of β lead to close to linear proportionality between these quantities as observed in Fig. 3 of the main article.

The somewhat smaller exponent in the temperature dependency of N_{100} compared to that of [MT] at all the sites seems reasonable for various reasons:

1) The direct anthropogenic particle emissions are relatively more significant at lower temperatures. The relatively high B_{100} values at Hohenpeisseberg and Yakutsk at temperatures between 0 and 10 °C (Figs. S1b and S1f), which are presumably related to anthropogenic emissions, seem to indicate anthropogenic emissions also as a reason for low values of β_N at these stations.

2) The particles growing into the studied size range are presumably better mixed within the BL than relatively short-living monoterpenes, which have sources on and near the surface. As the BL height typically increases with increasing temperature also this difference becomes more significant.

3) The larger N_{100} increases the coagulation sink of smaller particles, possibly slowing the increase in number of particles growing to 100 nm sizes.

4) The life-time of monoterpenes is short (~hour) and thus they follow the diurnal cycle of emissions exponentially related to temperature. The N_{100}, however, have a life-time of approximately 5 days and thus persist over the diurnal cycle. Accordingly, monoterpene concentrations vary with the diurnal temperature variation whereas particle concentration is also influenced by the conditions during the days before.

5) The evaporation rates of the semi-volatile organic vapours increase with increasing temperature, which possibly diminishes the fraction of molecules that remain in the particles out of all condensed molecules.

Details of the feedback calculation

Even though no comprehensive aerosol-climate simulation was done for the overall climate feedback strength, we estimated the order-of-magnitude of the feedback on the direct and first indirect (cloud albedo) effect. To do this, we first binned all the daily mean N_{100} concentrations to mean daily air temperature bins with a resolution of one degree Celsius. We then assumed that the effect from one degree warming could be evaluated by comparing the daily concentration to the concentration of the same percentile in the one degree warmer bin (Figure S6a-b). In other words, we assumed that the order of concentrations will stay the same, i.e. the day with e.g. the highest concentration in the current climate will also have the highest concentration in the one degree warmer climate. In the cases where there were no observations in the warmer temperature bin, no concentration change was assumed. The comparison with the higher temperature concentrations was also done for particle volume concentrations (for particle diameters < 500 nm, assuming spherical particles) to provide similar approximation of the change in particle volume on climate warming of 1K.

For the aerosol cloud albedo effect, we approximated the relative change of the cloud droplet number concentration ($\Delta N_d/N_d$) from the change in N_{100} number using a parameterization derived from eq. 14 in Gultepe and Isaac[57] (Fig S6c). The change in cloud albedo ΔA for that measurement day was then calculated from[58]:

$$\Delta A = \frac{A(1-A)\left[\left(1+\frac{\Delta N_d}{N_d}\right)^{1/3}-1\right]}{1+A\left[\left(1+\frac{\Delta N_d}{N_d}\right)^{1/3}-1\right]}, \qquad (2)$$

where A is the original cloud albedo. This equation is based on a two-stream approximation to radiative transfer, it assumes a homogeneous, conservatively scattering cloud layer and, most importantly, that neither cloud liquid water path nor the shape of the droplet size distribution (i.e., the ratio of volume-equivalent and effective radius) change with changing N_d. The local radiative feedback for this cloud albedo change was

$$\frac{\Delta F_i}{\Delta T} = -SCT_{at}^2 \Delta A \ , \qquad (3)$$

where C is the mean fractional low cloud cover, T_{at} is the atmospheric transmissivity (0.76), and S is the mean daily solar radiation flux at the top of the atmosphere for the day and location of the measurement.

The values of cloud cover were estimated from ISCCP D2 data for years 1984-2006[59]. We used the closest values in T21 resolution of the average low-cloud fraction, corrected for overlap by $C = C_{low}/(1-C_{mid}-C_{high})$, where C_{low}, C_{mid} and C_{high} are the monthly mean low, middle and high cloud cover of ISCCP database. If the cloud cover data for a measurement month was not available, the annual average value was used instead. For initial cloud albedo A, a uniform distribution between 0.3 and 0.8 was assumed, and the given value of forcing is the average of 100 random realizations.

The method applied for evaluating concentration differences can in some cases lead to outlier feedback values, as the temperature bins can have very few observations near the highest and lowest temperatures observed (Fig S6d). To remove the effect of the outliers on averages, we only used daily feedback values with an absolute value below 10 W m^{-2} K^{-1} to calculate annual averages, which removed less than 2% of the days from the analysis. The resulting local albedo feedbacks are presented in Fig. 4b in the main article.

For clean and moderately polluted background areas with all-year data, the feedback was in the range from -0.3 to +0.01 W m^{-2} K^{-1} (see Table S3), with mean value of -0.1 W m^{-2} K^{-1}. At the most polluted stations in this study, San Pietro Capofiume and K-Puszta, the feedback values were positive i.e. warming, because the aerosol concentrations decreased with increasing temperature for the most of the temperature range. This decrease is most likely due to the increasing of BLH with increasing temperature, causing more effective dilution of the emissions and thus lower concentrations at higher temperatures. The feedback varied at these stations from +0.02 to +0.07 W m^{-2} K^{-1} (mean +0.05 W m^{-2} K^{-1}). We also calculated the feedback values for the periods during which the daily mean temperature was over 5 °C to approximate the effect of growing season on the feedback. On the clean and moderately polluted background sites, this increased the magnitude of the cooling feedback significantly (note that Yakutsk data was only available for summertime) to -0.8 to +0.01 W m^{-2} K^{-1} (mean -0.3 W m^{-2} K^{-1}). At the polluted background sites almost no change was seen from annual averages. For the South African Botsalano station, the growth season is mostly determined by rainfall, and thus there was no change in the feedback from the temperature-based growth season.

In order to get rough global estimates of the impact of the aerosol climate feedback outside of polluted regions, we used an approximate value of 10% of the global area covered by either different types of forests (excluding rain forest) or croplands[27] and further assumed that the background values for clean and moderately polluted environments are representative for these regions. With these assumptions, the overall global feedback effect is of the order of magnitude of -0.01 W m^{-2} K^{-1}. The real value of feedback may be outside of the range obtained by this simple analysis, because *i*) the global estimates of the input parameters in the calculation are only approximated, *ii*) potential correlations between the relevant quantities involved could not be

taken into account, *iii*) no distinction between the boundary layer and free troposphere was made, *iv*) only the first indirect effect was considered[60], and *v)* the feedback could be affected by additional buffering effects in the aerosol-cloud interactions[30].

For the direct aerosol effect, we used the approach from Lihavainen *et al.*[61]. The temperature-induced change of 1 K warming in the daily mean aerosol volume concentration (assuming spherical particles) for particle diameters below 500 nm was calculated as in the indirect case, above. The change in aerosol volume burden B_V was then calculated with further assumption that the boundary layer height does not change significantly in one degree warming. Assuming that the change in the volume concentration was caused only by condensed organics with density of ρ=1.0 g cm^{-3} and mass extinction coefficient of B_{sp} = 3.9 m^2 g^{-1}, we then directly calculated the change in the optical depth

$$\Delta\tau = \Delta B_V \rho B_{sp} . \qquad (4)$$

By assuming unity single scattering albedo for the aerosol, we then calculated the change in the aerosol daily direct effect using (e.g, ref. 62)

$$\frac{\Delta F_d}{\Delta T} = -(\Delta\tau)\beta S \phi T_{at}^2 (1-C_c)(1-R_s)^2 , \qquad (5)$$

where β is the average upscatter fraction (assumed to be 0.3), Φ is the mean daytime value of the secant of the zenith angle, R_s is the surface albedo (set to 0.1) and C_c is the Cunningham slip correction factor. Averaging over the measurement periods, the range of changes in the direct effect could be then estimated (Fig 3b in the main article). The changes from one degree warming spanned the range from -0.04 to +0.006 W m^{-2} K^{-1}, with mean value of -0.02 W m^{-2} K^{-1} of regional feedback (see Table S3). Using the same global land area approximation as above, we estimate the magnitude of this feedback to be -0.002 W m^{-2} K^{-1}. These changes due to the

direct aerosol effect are at most of the stations roughly an order of magnitude smaller than those due to the cloud albedo effect.

One should note that the values for the feedback are calculated with air temperatures measured at continental stations, and as the continental climate is probably warming faster than the global mean, the feedback could be stronger at the global scale. The feedbacks are calculated for one degree change from the current climate, and the feedback strength will probably change in higher temperature differences, especially considering that there is no knowledge how the BVOC emissions will change in extreme climate conditions.

Supplementary Figures

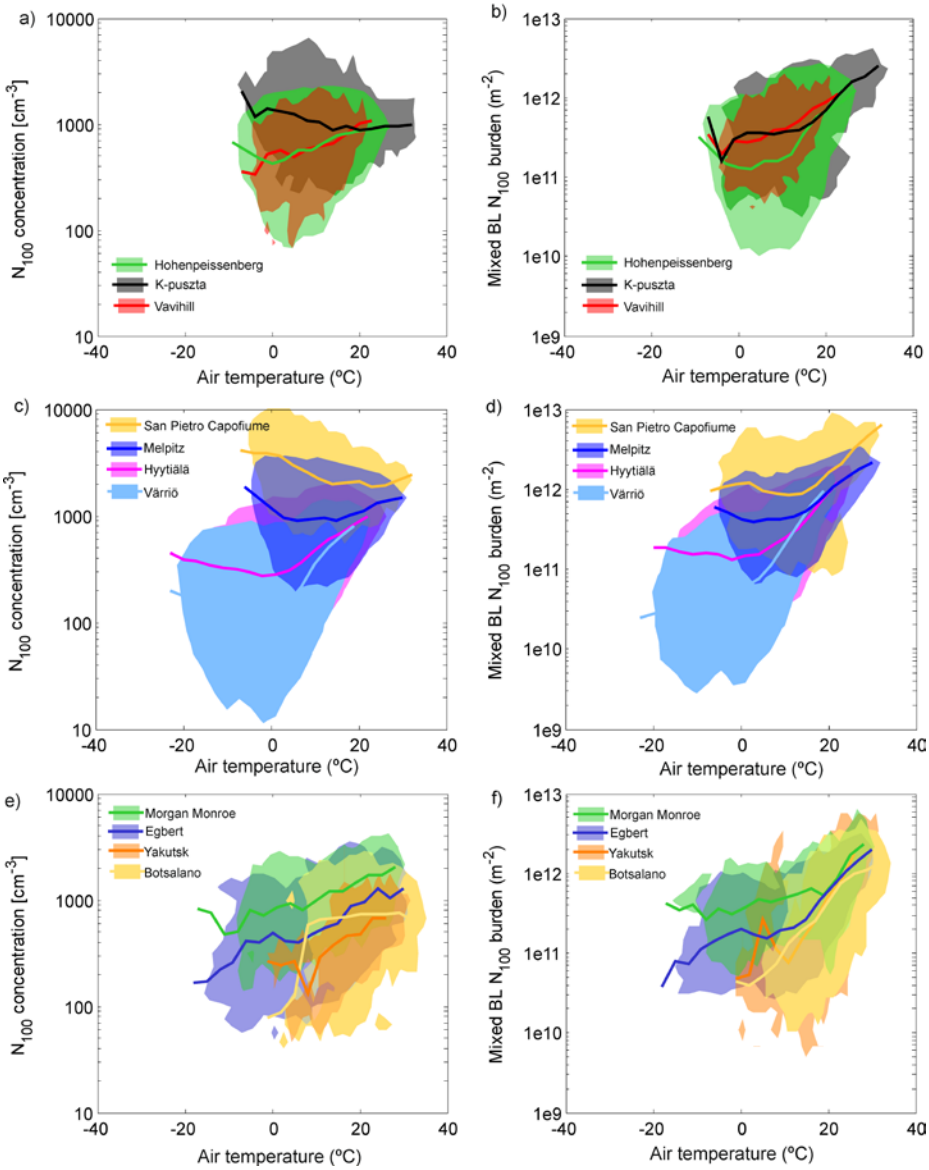

Fig. S1 a) Median number concentrations of over 100 nm particles at Hohenpeissenberg, K-puszta and Vavihill measurement stations as a function of air temperature. The shaded areas cover 95% of the observations. b) Same as a) but for (well mixed) boundary layer number burden B_{100}; c-d) same as a-b) but for San Pietro Capofiume, Melpitz, Hyytiälä and Värriö; e-f) same as a-b) but for Morgan Monroe, Egbert, Yakutsk and Botsalano.

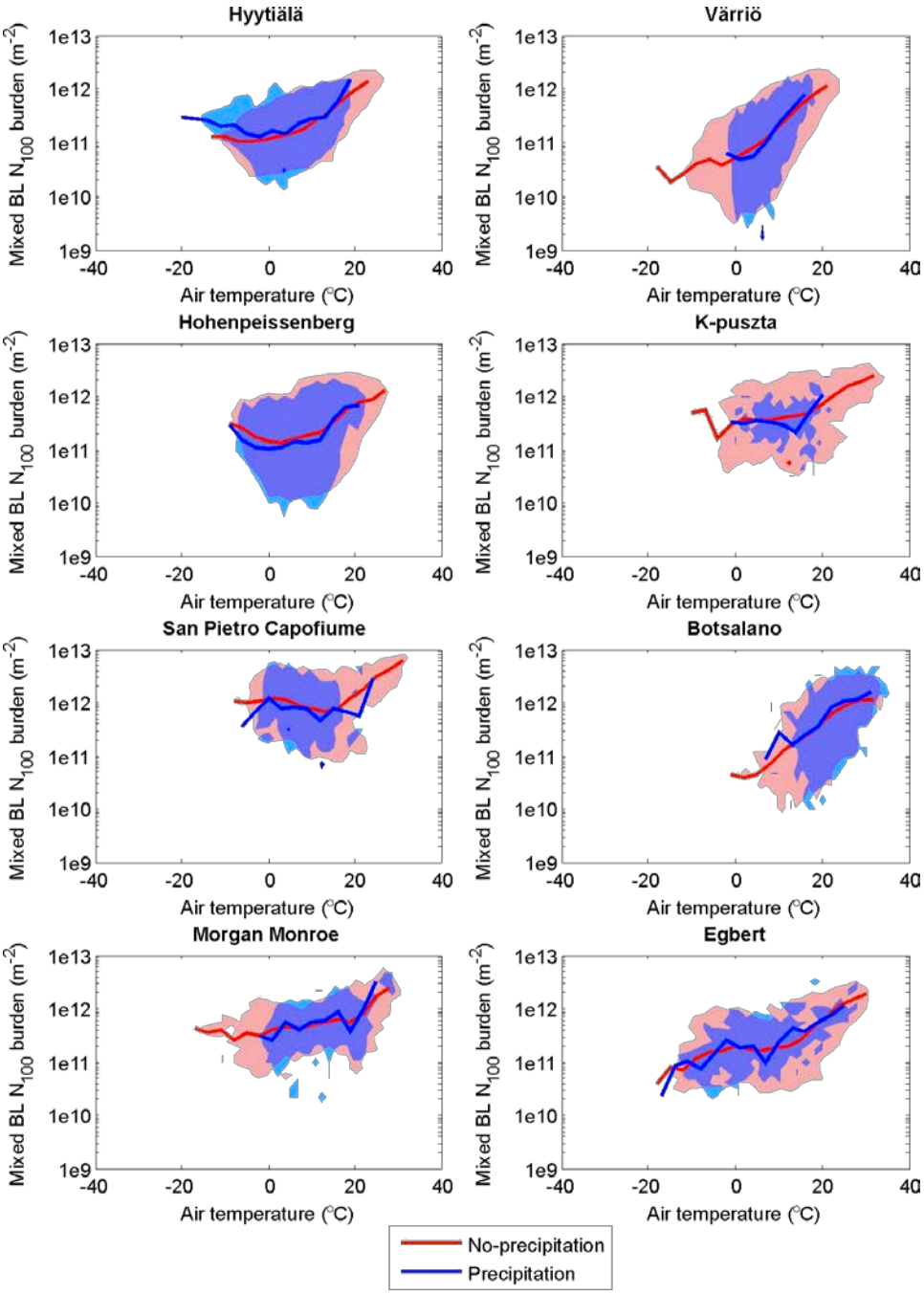

Fig. S2. The same figure and data as in Fig. 1c of the main article and Fig. S1 in supporting material, the data divided to periods with liquid precipitation (blue) and no-precipitation (red) periods, for those stations from which the precipitation data were available. The lines represent the median value in each temperature.

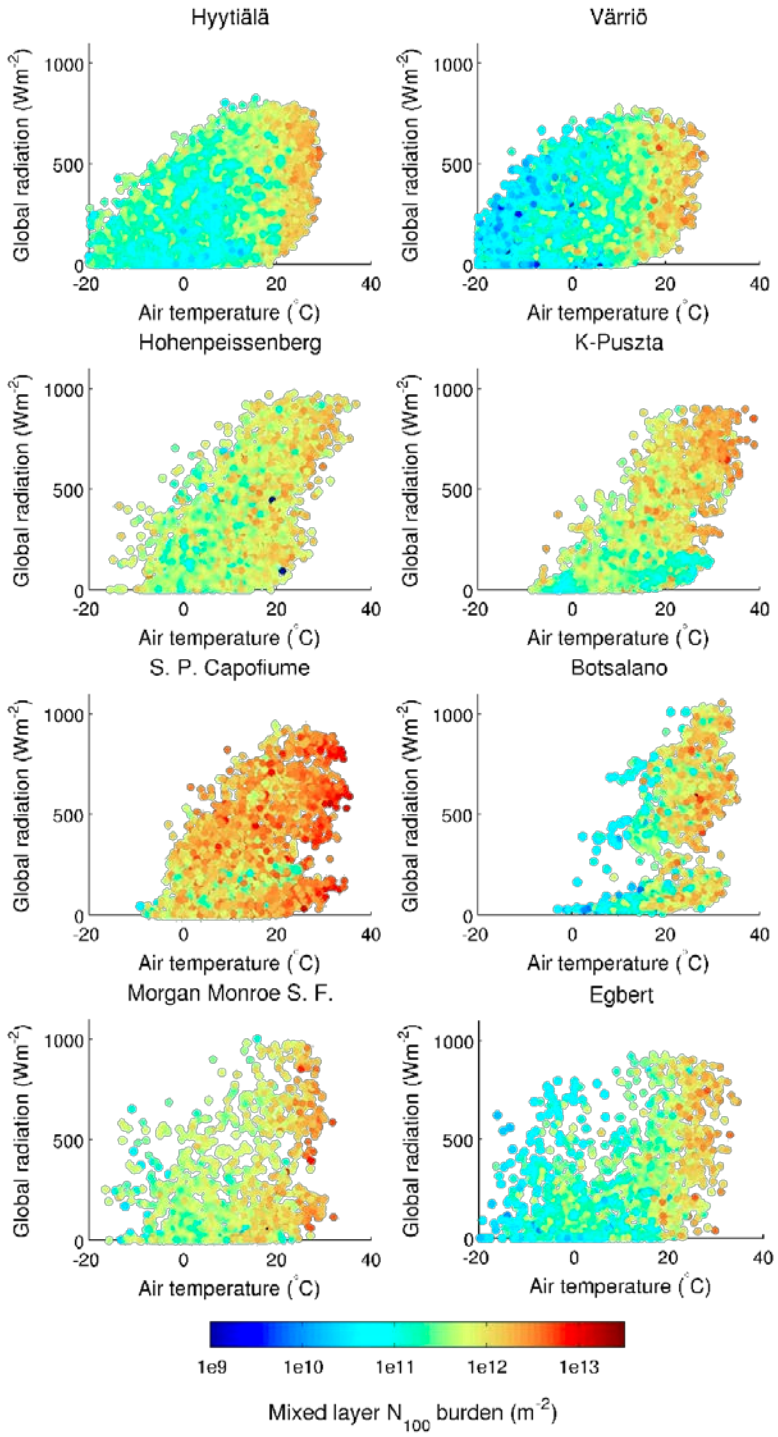

Fig. S3. Three hour averages (between 4:30 a.m. and 22:30 p.m.) of the mixed layer number burdens B_{100}, indicated with colour, presented versus temperature and global radiation at those sites from which the global radiation data was available.

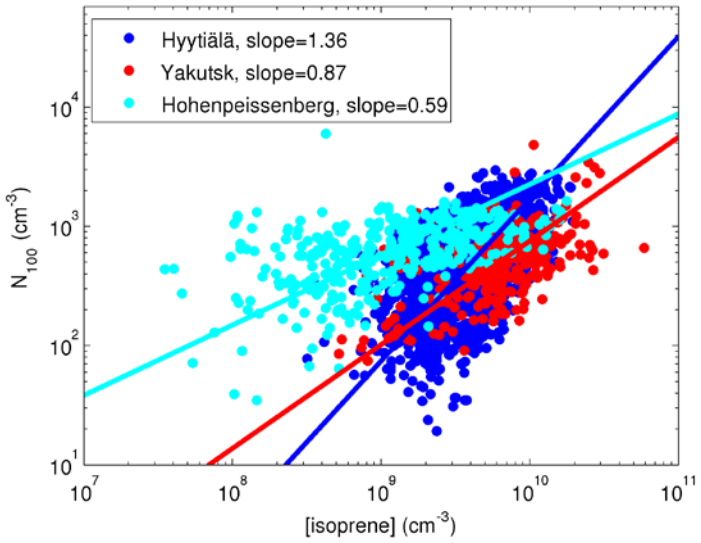

Fig. S4. Concentration N_{100} as a function of gas phase isoprene concentration. The comparison is for T > 5°C, at Hyytiälä the data covers 21 months and at Hohenpeissenberg 15 months from all the seasons, and at Yakutsk two months between May and August. The figure shows less uniform dependence of N_{100} on isoprene concentration than on monoterpene concentrations, the latter depicted in Fig. 3 of the main article.

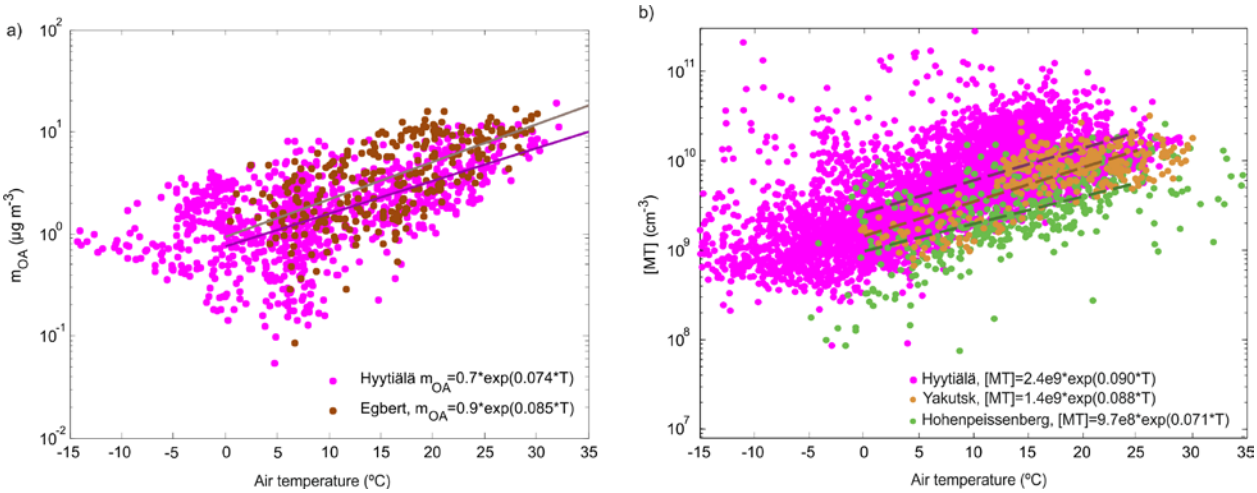

Fig. S5. a) Mass of organic compounds in AMS derived particle composition data as a function of temperature in two stations. b) Monoterpene concentration [MT] as a function of air temperature. Regression fits are made to data points with T > 0°C.

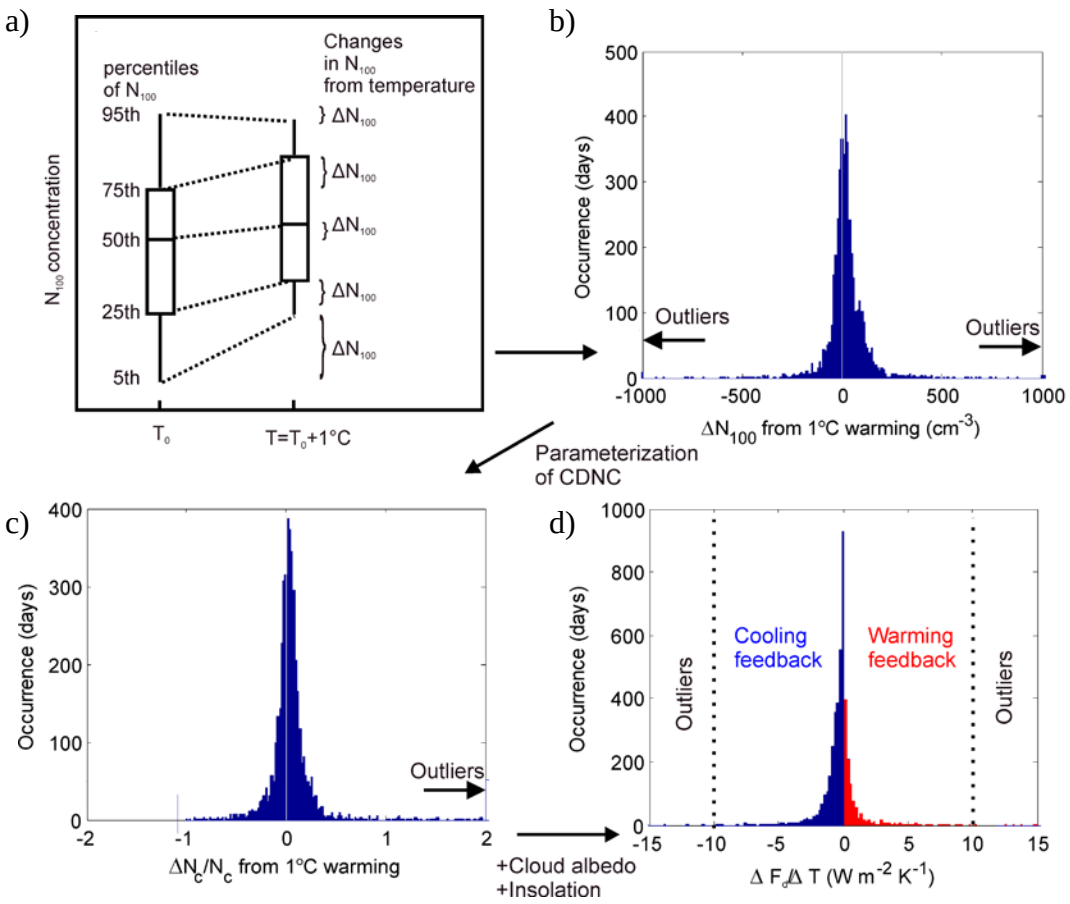

Fig. S6. Schematic representation of N_{100} concentration difference calculation. a) each daily average concentration was compared to similar percentile concentration in one degree warmer days and thus for each day an approximation of temperature-dependent ΔN_{100} was obtained. The value of ΔN_{100} due to one °C increase in temperature b) was more often positive than negative, i.e. temperature increase increased N_{100} concentrations. The method did, however, produce some extreme estimates of ΔN_{100}. c) Using the parameterization of Gultepe and Isaac[55] (eq. 14 of the cited article), the ΔN_{100} values were converted to relative changes of cloud droplet number concentrations, and d) using the equations 2 and 3 in Supplementary Methods derived into daily forcing estimates. In averaging the local forcing estimates the outlier values with $|\Delta F_d/T| > 10$ $Wm^{-2}K^{-1}$ were excluded.

Supplementary Tables

Table S1. *p*-values of the statistical tests done for log-linear slopes of either N_{100} or B_{100} with air temperature time series for temperatures above 5 °C. Bolded values are statistically significant with $p < 0.05$ significance level. See Supplementary Methods for details of the test.

	p (N_{100})	p (B_{100})
Hyytiälä	**<0.001**	**<0.001**
Värriö	**<0.001**	**<0.001**
Vavihill	**0.01**	**<0.001**
Hohenp.	**<0.001**	**<0.001**
Melpitz	**<0.001**	**<0.001**
K-Puszta	0.93	**<0.001**
Yakutsk	**<0.001**	**<0.001**
S. P. Cap.	0.99	**<0.001**
Botsalano	0.06	**<0.001**
M. Monroe	**<0.001**	**<0.001**
Egbert	**<0.001**	**<0.001**

Table S2. Results of the least squares regression fits (log to linear) to temperature dependencies of monoterpene concentrations ([MT]), organic aerosol mass (m_{OA}) and CCN-sized particle number concentration (N_{100}). The 95 % confidence intervals are given in parenthesis (see Supplementary Methods for details of calculation).

	β_{MT} in [MT] = α_{MT}*exp($\beta_{MT}T$/°C)	β_{OA} in m_{OA} = α_{OA}*exp(β_{OA} T/°C)	β_{N} in N_{100} = α_{N}*exp(β_{N} T/°C)
Hyytiala	0.090 (0.081 0.098)	0.074 (0.058 0.093)	0.085 (0.073 0.098)
Hohenpeissenberg	0.071 (0.058 0.083)	-	0.029 (0.020 0.037)
Yakutsk	0.088 (0.073 0.105)	-	0.033 (0.010 0.055)
Egbert	-	0.085 (0.066 0.107)	0.072 (0.053 0.093)

Table S3. Calculated feedback values in units W m^{-2} K^{-1}. Annual and growth season averages are presented, the latter determined by taking into account the days during which daily mean temperature was above 5 °C. In Yakutsk the data did not include a whole year, but only late spring and summer.

	Cloud albedo effect		Direct effect	
	Annual	$T > 5$°C	Annual	$T > 5$°C
Yakutsk		-0.46		-0.026
Egbert	-0.32	-0.51	-0.034	-0.060
Värriö	-0.25	-0.76	-0.019	-0.060
Hyytiälä	-0.13	-0.39	-0.017	-0.037
M. Monroe	-0.07	-0.06	-0.037	-0.052
Hohenp.	-0.05	-0.11	-0.006	-0.016
Melpitz	-0.03	-0.10	-0.005	-0.012
S. P. Cap.	0.02	0.02	-0.035	-0.049
Vavihill	-0.01	-0.08	-0.001	-0.002
Botsalano	0.01	0.01	-0.019	-0.019
K-Puszta	0.07	0.06	0.006	0.006
Average	**-0.08**	**-0.19**	**-0.02**	**-0.03**

Referenes:

31. Hari, P. & Kulmala, M. Station for Measuring Ecosystem-Atmosphere Relations (SMEAR II). *Boreal Env. Res.*, **10,** 315–322 (2005).

32. Hari, P, *et al*. Air pollution in eastern Lapland: challenge for an environmental measurement station. *Silva Fennica*, **28,** 1, 29–39 (1994).

33. Kristensson, A. *et al*. Characterization of new particle formation events at a background site in Southern Sweden: relation to air mass history. *Tellus B*, **60,** 330–344, doi:10.1111/j.1600-0889.2008.00345.x (2008).

34. Birmili, W., K *et al*. A case of extreme particulate matter concentrations over Central Europe caused by dust emitted over the southern Ukraine. *Atmos. Chem. Phys.*, **8,** 997-1016, (2008).

35. Birmili, W. *et al*. The Hohenpeissenberg aerosol formation experiment (HAFEX): a longterm study including size-resolved aerosol, H_2SO_4, OH, and monoterpenes measurements. *Atmos. Chem. Phys*., **3,** 361–376, doi:10.5194/acp-3-361-2003, (2003).

36. Kiss, G., Varga, B., Galambos, I., & Ganszky, I. Characterization of water-soluble organic matter isolated from atmospheric fine aerosol. *J. Geophys. Res*., **107,** 8339–8347, doi:10.1029/2001JD000603, (2002).

37. Hamed, A., *et al*. Nucleation and growth of new particles in Po Valley, Italy. *Atmos. Chem. Phys*., **7,** 355-376, doi:10.5194/acp-7-355-2007, (2007).

38. Ohta T., *et al*. Interannual variation of water balance and summer evapotranspiration in an eastern Siberian larch forest over a 7-year period (1998-2006). *Agric. For. Met.*, **148,** 1941-1953, (2008).

39. Pryor, S.C., Barthelmie, R.J. & Spaulding, A.M. New particle formation in the Midwestern USA: Event characteristics, meteorological context and vertical profiles. *Atmos. Environ.*, **44,** 4413-4425, (2010)

40. Slowik, J. G. *et al*. Characterization of a large biogenic secondary organic aerosol event from eastern Canadian forests. *Atmos. Chem. Phys*., **10,** 2825–2845, (2010)

41. Laakso, L., *et al*. Basic characteristics of atmospheric particles, trace gases and meteorology in a relatively clean Southern African Savannah environment. *Atmos. Chem. Phys*., **8,** 4823-4839, doi:10.5194/acp-8-4823-2008, (2008).

42. Oderbolz, D. C., *et al*. A comprehensive emission inventory of biogenic volatile organic compounds in Europe: improved seasonality and land-cover. *Atmos. Chem. Phys.*, **13**, 1689-1712, doi:10.5194/acp-13-1689-2013, (2013).

43. Otter, L., A., *et al.* Spatial and temporal variations in biogenic volatile organic compound emissions for Africa south of the equator. *J. Geophys. Res*., **108**, D13, 8505, doi:10.1029/2002JD002609, (2003).

44. Laj P. *et al.* Measuring atmospheric composition change. *Atmos. Environ*., **43,** 5351-5414 (2009).

45. Knutson, E. O. & Whitby, K. T. Aerosol Classification by Electric Mobility: Apparatus Theory and Applications. *J. Aerosol Sci*., **6,** 443–451, (1975).

46. Jeong, C.-H. & Evans, G. J. Inter-Comparison of a Fast Mobility Particle Sizer and a Scanning Mobility Particle Sizer Incorporating an Ultrafine Water-Based Condensation Particle Counter. *Aerosol Science and Technology,* **43,** 4, (2009)

47. Denier van der Gon, H., *et al*. Size-resolved Pan-European Anthropogenic Particle Number Inventory, paper presented at International Aerosol conference (oral), 29/8-3/9 2010,

Helsinki (2010).

48. Schaap, M., *et al*. LOTOS-EUROS: Documentation, TNO report B&O-A, 2005-297, Apeldoorn (2005).
49. Lindinger W, Hansel, A. & Jordan, A. On-line monitoring of volatile organic compounds by means of Proton-Transfer-Reaction Mass Spectrometry (PTR-MS) Medical applications, food control and environmental research. *International Journal of Mass Spectrometry and Ion Processes*, **173,** 191-241, (1998).
50. De Gouw, J. & Warneke, C. Measurements of volatile organic compounds in the earth's atmosphere using proton-transfer-reaction mass spectrometry. *Mass Spectrom. Rev.*, **26,** 223–257 (2007).
51. Taipale, R. *et al.* Technical Note: Quantitative long-term measurements of VOC concentrations by PTR-MS – measurement, calibration, and volume mixing ratio calculation methods. *Atmos. Chem. Phys*., **8,** 6681-6698 (2008)
52. Holst, T., *et al.* BVOC ecosystem flux measurements at a high latitude wetland site. *Atmos. Chem. Phys.*, **10,** 1617-1634, doi:10.5194/acp-10-1617-2010, (2010).
53. Plass-Dülmer, C. & Berresheim, H. in *The German Contribution to the WMO/GAW Program: Upon the 225th anniversary of GAW Hohenpeissenberg Observatory*. Edited by W. Fricke (GAW Report 167, WMO TD No. 1336, 2007).
54. Handisides, G.M., Plass-Dülmer, C., Gilge, S., Bingemer, S. & Berresheim, H. Hohenpeissenberg Photochemistry Experiment (HOPE 2000): Measurements and photostationary state calculations of OH and peroxy radicals. *Atmos. Chem. Phys*., **3,** 1565-1588, (2003).

55. Cantrell, C. A. Technical Note: Review of methods for linear least-squares fitting of data and application to atmospheric chemistry problems. *Atmos. Chem. Phys*., **8,** 5477–5487, (2008).

56. Mudelsee, M. *Climate Time Series Analysis: Classical Statistical and Bootstrap Methods* (Springer, Dordrecht, The Netherlands, 2010).

57. Gultepe, I., & Isaac, G. A. Scale Effects on Averaging of Cloud Droplet and Aerosol Number Concentrations: Observations and Models. *J. Climate*, **12,** 1268–1279, (1999)

58. Platnick, S., & Twomey, S. Determining the susceptibility of cloud albedo to changes in droplet concentration with the advanced very high resolution radiometer. *J. Appl. Meteorol*., **33,** 334–347, (1994).

59. Rossow, W. B. & Dueñas, E. N. The international satellite cloud climatology project (ISCCP) web site. *Bull. Amer. Met. Soc*, **85,** 167-172 (2004).

60. Kerminen, V.-M., Lihavainen, H., Komppula, M., Viisanen, Y., & Kulmala, M. Direct observational evidence linking atmospheric aerosol formation and cloud droplet activation. *Geophys. Res. Lett.*, **32,** L14803, doi:10.1029/2005GL023130, (2005).

61. Lihavainen, H., *et al*. Observational signature of the direct radiative effect by natural boreal forest aerosols and its relation to the corresponding first indirect effect. *J. Geophys. Res*., **114,** D20206, doi:10.1029/2009JD012078, (2009).

62. Sheridan, P. J., & Ogren, J. A. Observations of the vertical and regional variability of aerosol optical properties over Central and Eastern North America. *J. Geophys. Res*., **104,** 16,793-16,805, (1999).